bioRxiv preprint doi: https://doi.org/10.1101/2023.07.14.548877; this version posted October 23, 2023. The copyright holder for this preprint (which was not certified by peer review) is the author/funder, who has granted bioRxiv a license to display the preprint in perpetuity. It is made available under aCC-BY-NC-ND 4.0 International license.

Polysaccharide breakdown products drive degradation-dispersal cycles of foraging bacteria through changes in metabolism and motility

Astrid KM Stubbusch[1,2,3], Johannes M. Keegstra[4], Julia Schwartzman[5,6], Sammy Pontrelli[7], Estelle E. Clerc[4], Roman Stocker[4], Cara Magnabosco[3], Olga T. Schubert[1,2], Martin Ackermann[1,2,8], Glen G D'Souza[1,2]

[1]Institute of Biogeochemistry and Pollutant Dynamics, Department of Environmental Systems Science, ETH Zurich, Zurich, Switzerland
[2]Department of Environmental Microbiology, Eawag: Swiss Federal Institute of Aquatic Science and Technology, Duebendorf, Switzerland
[3]Geological Institute, Department of Earth Sciences, ETH Zurich, Zurich, Switzerland
[4]Institute of Environmental Engineering, Department of Civil, Environmental and Geomatic Engineering, ETH Zurich, Zurich, Switzerland
[5]Department of Civil and Environmental Engineering, MIT, Cambridge, MA, USA
[6]Department of Biology, University of Southern California, Los Angeles, USA
[7]Institute of Molecular Systems Biology, Department of Biology, ETH Zurich, Zurich, Switzerland
[8]Laboratory of Microbial Systems Ecology, School of Architecture, Civil and Environmental Engineering (ENAC), École Polytechnique Fédéral de Lausanne (EPFL), Lausanne, Switzerland

ORCID:
GD: 0000-0002-9123-101X
AS: 0000-0003-4767-2712
JK: 0000-0002-8877-4881
JS: 0000-0003-4563-4835
EC: 0009-0003-6046-2856
SP: 0000-0001-6265-8842
RS: 0000-0002-3199-0508
CM: 0000-0001-6871-7188
MA: 0000-0003-0087-4819
OS: 0000-0002-2613-0714

Corresponding authors: Glen G D'Souza and Astrid KM Stubbusch
Address: Eawag, Ueberlandstrasse 133, 8600 Duebendorf, Switzerland
Email: glengeralddsouza@gmail.com, astubbusch@icloud.com
Phone: +41-58-765-5495

Keywords: cooperative polysaccharide degradation, colony formation, cell dispersal, glycan, alginate, exoenzymes, alginate lyases, *Vibrio cyclitrophicus* ZF270

bioRxiv preprint doi: https://doi.org/10.1101/2023.07.14.548877; this version posted October 23, 2023. The copyright holder for this preprint (which was not certified by peer review) is the author/funder, who has granted bioRxiv a license to display the preprint in perpetuity. It is made available under aCC-BY-NC-ND 4.0 International license.

Abstract

Most of Earth's biomass is composed of polysaccharides. During biomass decomposition, polysaccharides are degraded by heterotrophic bacteria as a nutrient and energy source and are thereby partly remineralized into CO_2. As polysaccharides are heterogeneously distributed in nature, following the colonization and degradation of a polysaccharide hotspot the cells need to reach new polysaccharide hotspots. Even though these degradation-dispersal cycles are an integral part in the global carbon cycle, we know little about how cells alternate between degradation and motility, and which environmental factors trigger this behavioral switch. Here, we studied the growth of the marine bacterium *Vibrio cyclitrophicus* ZF270 on the abundant marine polysaccharide alginate. We used microfluidics-coupled time-lapse microscopy to analyze motility and growth of individual cells, and RNA sequencing to study associated changes in gene expression. Single cells grow at reduced rate on alginate until they form large groups that cooperatively break down the polymer. Exposing cell groups to digested alginate accelerates cell growth and changes the expression of genes involved in alginate degradation and catabolism, central metabolism, ribosomal biosynthesis, and transport. However, exposure to digested alginate also triggers cells to become motile and disperse from cell groups, proportionally increasing with the group size before the nutrient switch, accompanied by high expression of genes involved in flagellar assembly, chemotaxis, and quorum sensing. The motile cells chemotax toward alginate hotspots, likely enabling cells to find new polysaccharide hotspots. Overall, our findings reveal the cellular mechanisms underlying bacterial degradation-dispersal cycles that drive remineralization in natural environments.

Importance

Polysaccharides, also known as glycans, are the most abundant form of biomass on Earth and understanding how they are degraded by microorganisms is essential for our understanding of the global carbon cycle and the storage and release of CO_2 by natural systems. Although group formation is a common strategy used by bacterial cells to degrade ubiquitous polymeric growth substrates in nature, where nutrient hotspots are heterogeneously distributed, little is known about how cells prepare for dispersal from an exhausted nutrient source and re-initiate degradation of new nutrient patches. By

bioRxiv preprint doi: https://doi.org/10.1101/2023.07.14.548877; this version posted October 23, 2023. The copyright holder for this preprint (which was not certified by peer review) is the author/funder, who has granted bioRxiv a license to display the preprint in perpetuity. It is made available under aCC-BY-NC-ND 4.0 International license.

quantifying growth, motility and chemotaxis of individual cells and comparing gene expression changes when populations were exposed to either polysaccharides or their degradation products in the form of digested polysaccharides, we show that bacterial cells alter their behavior when they experience a shift from polymeric to digested polysaccharides: After cells form groups during growth on polymers, the exposure to degradation products made cells motile, enabling dispersal from sessile cell groups and - guided by chemotaxis - movement towards new polysaccharide hotspots. Our study sheds light on the cellular processes that drive bacterial growth and behavior during carbon remineralization, an important driver of CO_2 release from biomass in natural systems.

Introduction

Polysaccharides represent the largest fraction of biomass on Earth[1,2] and are constantly degraded and remineralized by microorganisms. Polysaccharides, also known as glycans, are long chains of monosaccharide units produced by cells for structural support (e.g., cellulose, chitin, and alginate) or energy storage (e.g., starch or glycogen)[1]. Heterotrophic microbes obtain nutrients and energy from the polysaccharide breakdown products. They often use exoenzymes, either secreted or anchored in the cell membrane[2,3], to cleave these large polymers into smaller units that can be taken up by cells. The formation of dense cell groups is observed during growth on polysaccharides by diverse bacteria, including the soil- and gut-dwelling *Bacillus subtilis*[3], the oligotrophic fresh-water *Caulobacter crescentus*[4], and several representatives of the copiotrophic[5,6] marine *Vibrio spp.*[7,8]. It has been suggested that "cooperative" growth[3], where dense cell groups reduce diffusional loss of valuable degradation products and secreted exoenzymes, represents a general principle in polysaccharide degradation[4,8]. Yet, how bacteria subsequently disperse from exhausted polysaccharide sources and navigate towards new polysaccharide hotspots remains poorly understood.

To study the cellular mechanisms that govern the switch between polysaccharide degradation and dispersal toward new polysaccharide hotspots, we worked with the ubiquitous marine Gammaproteobacterium *Vibrio cyclitrophicus* ZF270, a degrader of the prevalent marine polysaccharide alginate[6,9]. Alginate is a linear polysaccharide that is produced by brown algae as a cell

bioRxiv preprint doi: https://doi.org/10.1101/2023.07.14.548877; this version posted October 23, 2023. The copyright holder for this preprint (which was not certified by peer review) is the author/funder, who has granted bioRxiv a license to display the preprint in perpetuity. It is made available under aCC-BY-NC-ND 4.0 International license.

wall component, as well as by certain bacteria[10]. It can be cleaved into oligomers by endo-acting alginate lyases or into monomers by exo-acting alginate lyases (alginate lyases reviewed here[11]), namely β-D-mannuronic acid and α-L-guluronic acid[10]. *V. cyclitrophicus* ZF270 is found predominantly in the large-particle fractions of coastal water[12], can attach and form biofilms on the surfaces of multiple polysaccharides including alginate[13], and was shown to secrete alginate lyases during alginate degradation[8]. In this study, we used microfluidics coupled to automated time-lapse imaging to quantify the growth dynamics, group formation, and motility of *V. cyclitrophicus* ZF270 at the single-cell level under constant supply of either polymeric alginate or alginate degradation product in the form of digested alginate, as well as upon a transition from alginate to digested alginate. Furthermore, we used RNA-sequencing to compare the gene expression of *V. cyclitrophicus* ZF270 grown on alginate and digested alginate. We found striking responses to the form of alginate in growth rate, group formation, motility and chemotaxis, as well as in the expression of corresponding genes. Overall, our work provides insights into the metabolic and cellular regulation that allows cells to forage in heterogeneous nutrient-scapes through degradation-dispersal cycles.

Results

Extracellular break down of alginate delays population growth

To probe the phenotypic and metabolic regulation of bacterial cells during the progressive degradation of a polysaccharide source, we developed an experimental system consisting of the marine bacterium *V. cyclitrophicus* ZF270 growing on alginate, a highly abundant polysaccharide in the ocean. To mimic the local nutrient environment during the colonization of a new polysaccharide source, we used 0.1% weight per volume (w/v) algae-derived alginate in its soluble form (in the following also simply referred to as "alginate"). Since commercially available alginate breakdown products of specific sizes are limited and expensive, with only one monomeric component available at a considerable cost, we simulate an advanced stage of polysaccharide degradation by supplying cells with digested alginate (0.1% (w/v)). This digested alginate is prepared by treating alginate with a readily available endo-acting alginate lyase (see Materials and Methods). This mimics an environment where degradation products like monomers and oligomers become abundant through the action of extracellular alginate lyases. The commercially

bioRxiv preprint doi: https://doi.org/10.1101/2023.07.14.548877; this version posted October 23, 2023. The copyright holder for this preprint (which was not certified by peer review) is the author/funder, who has granted bioRxiv a license to display the preprint in perpetuity. It is made available under aCC-BY-NC-ND 4.0 International license.

available alginate lyase has been shown to produce alginate oligomers of progressively smaller size over extended digestion periods[14,15]. We used Liquid Chromatography-Mass Spectrometry (LC-MS) to analyze the composition of the digested alginate, which had been subject to 48 hours of digestion. We found that digested alginate contained more monosaccharides than untreated alginate, which contained more alginate molecules of higher molecular weight (Fig. S1).

Using this system, we first set out to investigate the growth dynamics of *V. cyclitrophicus* ZF270 in well-mixed batch cultures containing either alginate or digested alginate as a sole carbon source (Fig. S2A). We found that similar yields were reached in the alginate and digested alginate cultures as indicated by optical density (Fig. S2B and C) and confirmed by colony counts (Fig. S3), suggesting that the same amount of alginate supports a similar yield irrespective of its degree of depolymerization. However, the onset of growth on alginate was delayed by about 7.5 hours compared to growth on digested alginate (Fig. S2D and E). This is consistent with previous observations that in well-mixed environments the lag time of bacteria growing on alginate can be reduced by the external supplementation of alginate lyases[8,14]. Together, these findings indicate that growth on polysaccharides such as alginate in well-mixed cultures is initially limited by the extracellular breakdown of the polysaccharide.

Large cell groups form on alginate but not on digested alginate

To better understand how cells react to the changing degree of depolymerization of a polysaccharide source during degradation, we investigated the growth of *V. cyclitrophicus* ZF270 at the level of single cells on alginate and digested alginate. For this purpose, we grew the cells in microfluidic growth chambers, described in detail by Dal Co et al.[16], where cells were provided with a continuous flow of culture media containing either alginate or digested alginate as carbon source. We found that over 24 hours dense groups of more than 1000 cells formed on alginate, filling the entire microfluidic chamber (Fig. 1A). In contrast, cells supplied with digested alginate grew in smaller groups that never exceeded 100 cells per chamber (Fig. 1B and C). Reconstructed cell lineages revealed that the large cell groups on alginate formed because cells often did not disperse after division and thereby formed dense cell

bioRxiv preprint doi: https://doi.org/10.1101/2023.07.14.548877; this version posted October 23, 2023. The copyright holder for this preprint (which was not certified by peer review) is the author/funder, who has granted bioRxiv a license to display the preprint in perpetuity. It is made available under aCC-BY-NC-ND 4.0 International license.

153 groups originating from a single cell lineage (Fig. 1A). The lower cell density on digested alginate could
154 be caused by slower growth or by more cells leaving the chambers. As the maximum growth rate both
155 in bulk and on single cell level is similar in alginate and digested alginate (Fig. S2E and F), it is most
156 likely that the lower cell density in digested alginate is caused by cell dispersal. These observations
157 suggest that cells can modulate their propensity to form groups depending on the state of polysaccharide
158 degradation in their local environment. Similar observations were made with a different model system
159 (*Caulobacter crescentus* growing on the polysaccharide xylan)[14], indicating that group formation on
160 polymeric nutrient sources may be a general mechanism of bacteria that degrade polysaccharides
161 extracellularly.
162

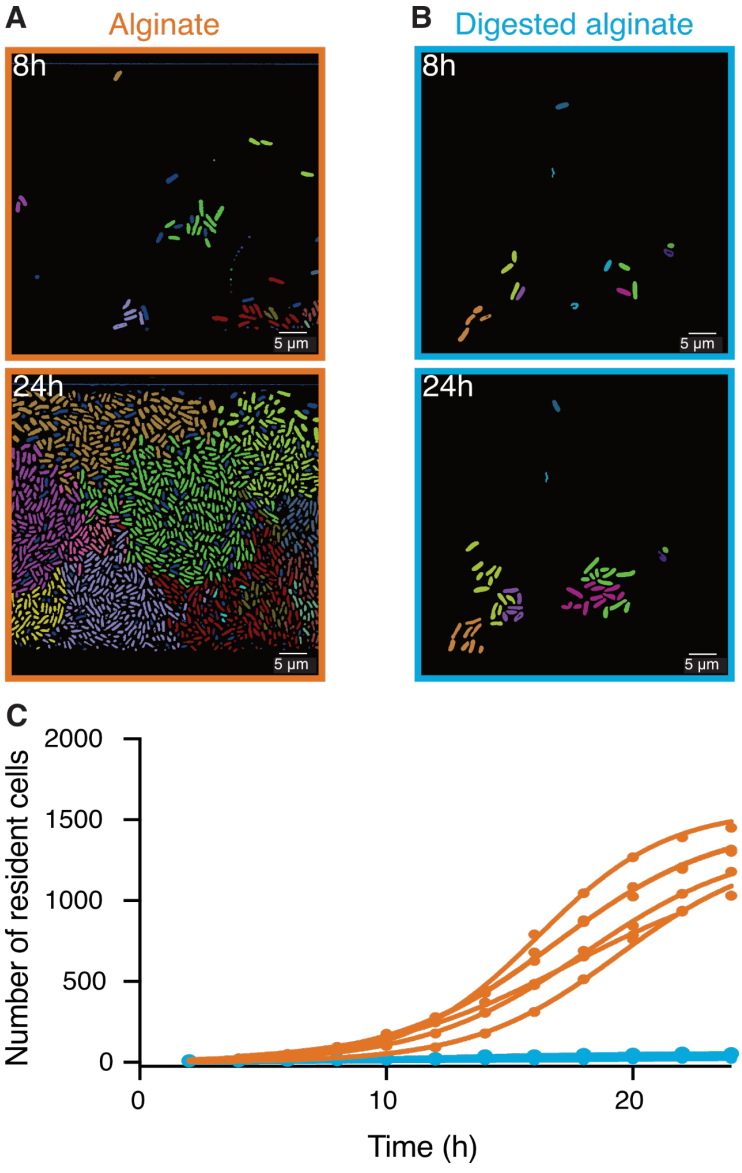

163

bioRxiv preprint doi: https://doi.org/10.1101/2023.07.14.548877; this version posted October 23, 2023. The copyright holder for this preprint (which was not certified by peer review) is the author/funder, who has granted bioRxiv a license to display the preprint in perpetuity. It is made available under aCC-BY-NC-ND 4.0 International license.

Figure 1. Large cell groups form on alginate but not on digested alginate. Representative images at different time points of *V. cyclitrophicus* ZF270 cells growing in microfluidic chambers, described in detail by Dal Co et al.[16], with (A) alginate medium or (B) digested alginate medium, both in their soluble form (not visible). Cells are false-colored according to their lineage identities based on cell segmentation and tracking over 24 hours. Cells without identified progenitors are colored in dark blue. See Supplemental Videos S1 (alginate) and S2 (digested alginate) for time-lapse videos. (C) Cell numbers within microfluidic chambers supplied with alginate (orange) are substantially higher than cell numbers within microfluidic chambers supplied with digested alginate (blue) (Logistic growth regression for alginate: R^2 = 0.99, maximal number of cells = 1217-1564, k = 0.24-0.38 h^{-1}; for digested alginate: R^2 = 0.86-0.97, maximal number of cells = 47-100, k = 0.07-0.4 h^{-1}). Circles indicate the number of cells present at a given time point in each chamber ($n_{chambers}$ = 7). Data for chambers with alginate originate from D'Souza et al.[8]. Lines are fits of a logistic growth regression line for each condition.

Transition from alginate to digested alginate triggers density-dependent dispersal of cells

To investigate the transition from the large cell groups formed on alginate to the small groups formed on digested alginate, we subjected *V. cyclitrophicus* ZF270 cells grown on alginate to a switch to digested alginate (Fig. 2A). Following the limited cell motility on alginate, this switch led to a rapid decrease in cell density within the growth chambers (Fig. 2B), presumably caused by cell dispersal. As we previously reported for other *Vibrionaceae* isolates, the growth rate of the cells on alginate was dependent on the local cell density: Initially the growth rate increased with cell density but then decreased at high cell densities, indicating that cell groups can benefit from the sharing of breakdown products generated by each other's exoenzymes, but also increasingly compete for nutrients[8]. This led us to investigate whether cell in larger groups, potentially experiencing stronger nutrient competition, might have a higher propensity to disperse after a switch to digested alginate than cells in smaller groups. We indeed found an inverse relationship between the number of cells at the time of the nutrient switch and the following change in cell number, meaning that cells in chambers with many cells were more likely to disperse than cells in chambers with less cells (Fig. 2C). Thus, during the transition from polysaccharides to degradation products, we found that the dispersal rate of cells depends on the size of the cell groups, likely through increased motility of cells in large groups.

bioRxiv preprint doi: https://doi.org/10.1101/2023.07.14.548877; this version posted October 23, 2023. The copyright holder for this preprint (which was not certified by peer review) is the author/funder, who has granted bioRxiv a license to display the preprint in perpetuity. It is made available under aCC-BY-NC-ND 4.0 International license.

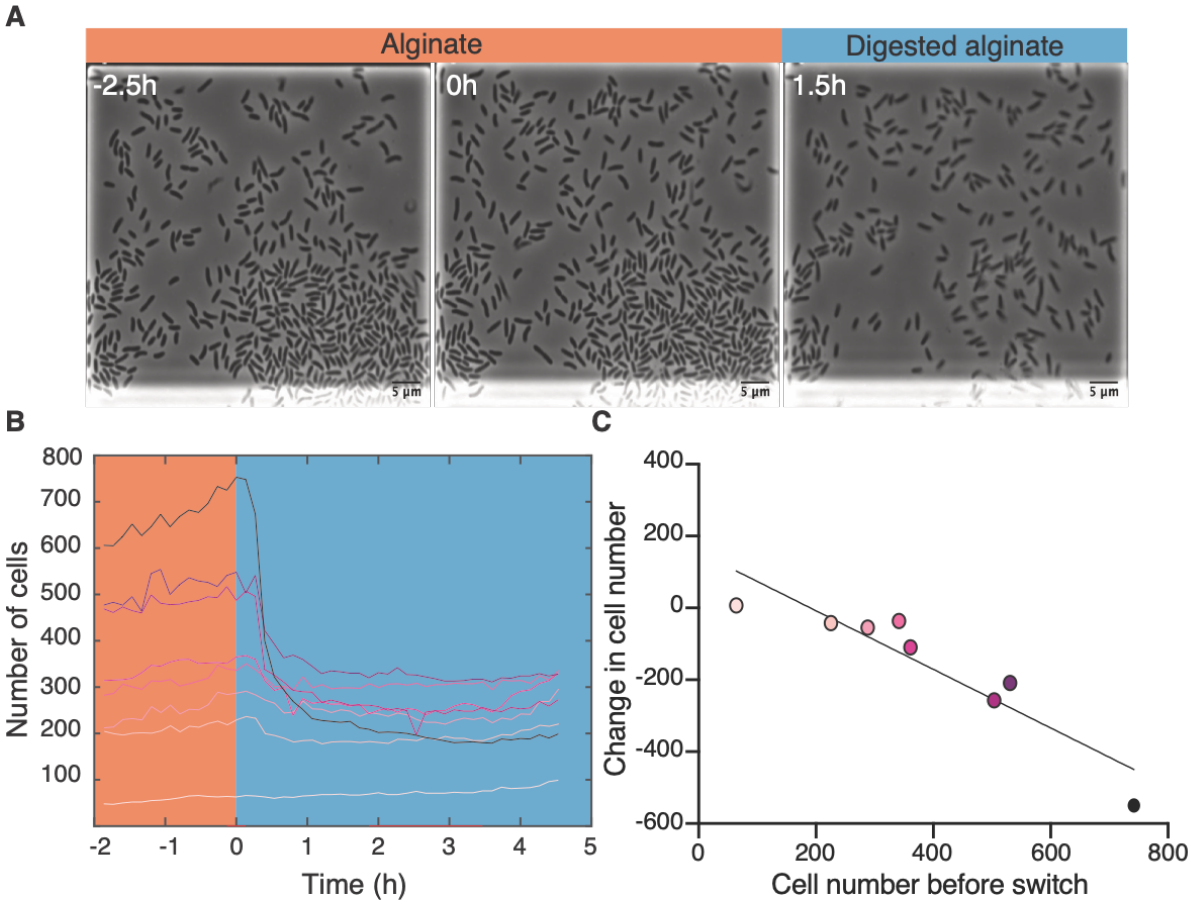

Figure 2. Transition from alginate to digested alginate triggers density-dependent dispersal of cells. (A) Representative time-lapse images of *V. cyclitrophicus* ZF270 cells (phase contrast microscopy) in microfluidic growth chambers that were initially exposed to alginate and then switched to digested alginate. (B) Number of cells in different chambers over time, each chamber indicated by a unique color (n = 8). The carbon source is indicated by the colored background (orange: alginate; blue: digested alginate). See Supplemental Video 3 for a time-lapse video. (C) Negative relationship between the difference in number of cells within the microfluidic growth chambers before and after the nutrient switch. Each circle represents one growth chamber with colors corresponding to (B), and the line depicts a linear regression fit (R^2 = 0.85, slope = -0.81, p-value < 0.001).

Cells growing on digested alginate are more motile and chemotax towards new polysaccharide sources

To investigate whether increased cell motility of *V. cyclitrophicus* ZF270 underlies the dispersal of cells observed after a shift to digested alginate, as also previously observed for *C. crescentus* cells on the monosaccharide xylose[4,14], we quantified the motility of single cells supplied with either alginate or digested alginate. We found that the single-cell swimming speed as well as the swimming distance were

bioRxiv preprint doi: https://doi.org/10.1101/2023.07.14.548877; this version posted October 23, 2023. The copyright holder for this preprint (which was not certified by peer review) is the author/funder, who has granted bioRxiv a license to display the preprint in perpetuity. It is made available under aCC-BY-NC-ND 4.0 International license.

significantly larger for cells supplied with digested alginate compared to cells supplied with alginate, and that a larger fraction of cells was motile (Fig. 3). This confirmed increased motility as a cellular response to the exposure to degradation products in the form of digested alginate.

To understand if the motile cells are directed by chemotaxis, we measured the chemotactic strength towards alginate and digested alginate using the In Situ Chemotaxis Assay (ISCA)[17,18]. We found *V. cyclitrophicus* ZF270 to significantly chemotax toward alginate (chemotactic index $I_c > 1$) but not toward digested alginate (Fig. 3F). This suggested that the increase in motility is accompanied by chemotaxis toward alginate. Overall, these findings suggest that once the breakdown of a polysaccharide source makes breakdown products available in the local environment, a fraction of cells becomes motile and disperses. These motile cells are guided by chemotaxis towards new polysaccharide sources, allowing them to start a new degradation-dispersal cycle.

Altered gene expression in central carbon metabolism, enzyme production, secretion and transporters, motility, and quorum sensing underlies the late-stage alginate degradation and cell dispersal

Next, we sought to elucidate the molecular mechanisms underlying the observed phenomenological disparities between cells cultivated on alginate and digested alginate. Due to the challenge of generating knock-out mutants in natural isolates, we used transcriptomics to investigate the differentially expressed genes of *V. cyclitrophicus* ZF270 under these respective conditions. To obtain a high-quality reference genome of *V. cyclitrophicus* ZF270, we sequenced and assembled a new reference genome using combined short and long read sequencing (BioProject PRJNA991487). We then grew cultures on either alginate or digested alginate until mid-exponential phase. To understand which cellular functions were affected by the expression changes, we first performed differential gene expression analysis using the software DESeq2. Here, genes exhibiting a log2 fold expression change greater than 0.5 or smaller than -0.5 between the two conditions, with a Benjamini-Hochberg(BH)-adjusted *p*-value below 0.01, were considered to be differentially expressed (Table S1). Next, we investigated which KEGG categories

bioRxiv preprint doi: https://doi.org/10.1101/2023.07.14.548877; this version posted October 23, 2023. The copyright holder for this preprint (which was not certified by peer review) is the author/funder, who has granted bioRxiv a license to display the preprint in perpetuity. It is made available under aCC-BY-NC-ND 4.0 International license.

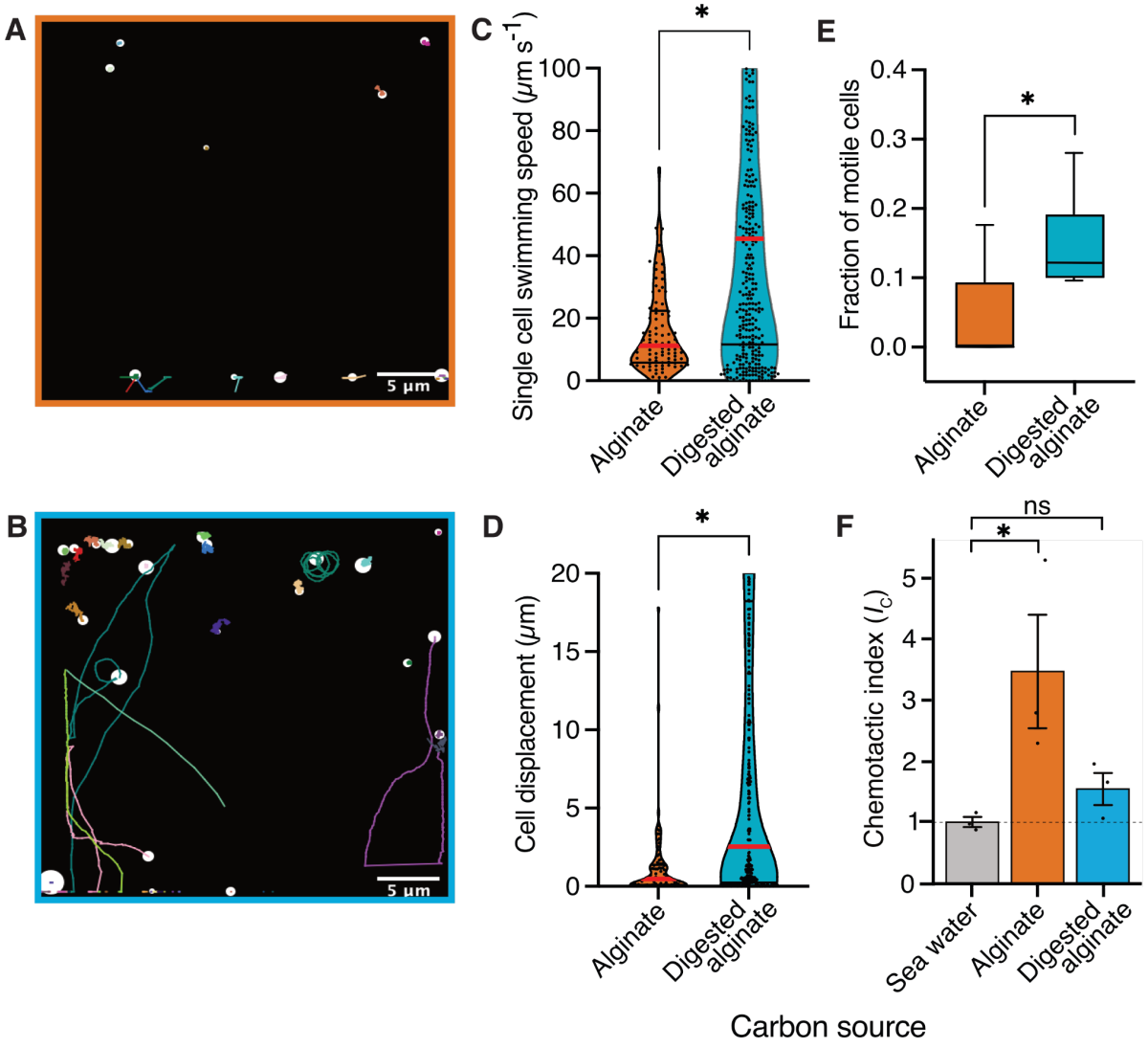

Figure 3. Cells are more motile on digested alginate than alginate and show chemotaxis towards alginate. (A and B) Spatial trajectories of cells supplied with (A) alginate or (B) digested alginate in representative microfluidic growth chambers are shown. White circles mark the starting point of each trajectory and colored lines mark the individual trajectories. (C) Distributions of the mean single-cell swimming speeds (Nested t-test, p-value < 0.0007, t = 4.803, df = 10, n_{cells} = 86 vs 375 in $n_{chambers}$ = 5) are shown. (D) Distributions of cell displacement over the course of a trajectory (Nested t-test test, p-value < 0.0131, t = 4.39, df = 10, n_{cells} = 86 vs 375, and $n_{chambers}$ = 5) are shown. In (C) and (D) the red horizontal lines indicate the mean while black lines depict the 25th and 75th quartiles of the distribution. (E) The mean fraction of motile cells in each chamber, where motile cells are defined as cells with displacement greater than 1 µm (Mann-Whitney test on the means of five growth chambers, p-value = 0.034). In C, D, and E, each chamber was considered as an independent replicate. (F) Chemotactic index (I_C) quantified by In Situ Chemotaxis Assay (ISCA) (Tukey multiple comparisons of means,

bioRxiv preprint doi: https://doi.org/10.1101/2023.07.14.548877; this version posted October 23, 2023. The copyright holder for this preprint (which was not certified by peer review) is the author/funder, who has granted bioRxiv a license to display the preprint in perpetuity. It is made available under aCC-BY-NC-ND 4.0 International license.

95% family-wise confidence levels as error bars, p-value < 0.05, n = 3). Asterisks indicate statistically significant differences. See Supplemental Videos S4 and S5 for time-lapse videos of swimming cells.

were enriched in either genes with increased or decreased expression via Gene Set Enrichment Analysis (GSEA)[19] (Table S2) and found nine categories significantly enriched in genes with increased gene expression on digested alginate, and three categories significantly enriched in genes with decreased gene expression (Fig. 4A).

Cells growing on digested alginate showed expression changes in parts of the central metabolism and translation, compared to cells growing on alginate. Specifically, two pathways of the central metabolism were significantly enriched in genes with lower expression on digested alginate ("Valine, leucine and isoleucine biosynthesis" and "Propanoate metabolism" with a negative normalized enrichment score (NES), Fig. 4A, S4A and B, Table S3 and S4). We also found the gene set that encodes ribosomal proteins significantly enriched with genes highly expressed on digested alginate (positive NES, Fig. 4A and S4C, Table S5). This implies that cells invest proportionally more of their transcriptome into the production of new proteins, a sign of faster growth[20,21]. Both observations likely relate to the different growth dynamics of *V. cyclitrophicus* ZF270 on digested alginate compared to alginate.

The expression of transporters and secretion systems was generally increased in cells growing on digested alginate, compared to cells growing on alginate. This includes genes with a function in "Bacterial secretion systems", namely secretion systems I to VI, which mediate protein export through the inner and outer membranes of Gram-negative bacteria (Fig. 4A and S4D, Table S6). Notably, eleven of the thirteen General Secretion Pathway (GSP) genes (part of the type II secretion system) showed 1.1 to 3.4-fold increased expression levels on digested alginate (p-values < 0.01, Fig. 4A, Table S8). The GSP is known to facilitate secretion of various extracellular enzymes like chitinases, proteases, and lipases[22,23], therefore, the positive enrichment on digested alginate may be linked to the export of extracellular alginate lyases. The KEGG BRITE category "Secretion system" was also enriched on digested alginate (Fig. 4A and S4D, Table S7). It contains additional genes involved in protein export,

bioRxiv preprint doi: https://doi.org/10.1101/2023.07.14.548877; this version posted October 23, 2023. The copyright holder for this preprint (which was not certified by peer review) is the author/funder, who has granted bioRxiv a license to display the preprint in perpetuity. It is made available under aCC-BY-NC-ND 4.0 International license.

of which especially genes of type IV pilus assembly, conjugal transfer pilus assembly, and MSHA pilus biogenesis were highly expressed on digested alginate, implicating them as interesting subjects to further research in their role in protein secretion and cell attachment and detachment during degradation-dispersal cycles of polysaccharide-degrading bacteria. Also, the gene set of transporters and in particular ABC transporters were positively enriched (Fig. 4A, Table S10 and S11). The latter showed enrichment especially in genes related to saccharide, iron, zinc, and phosphate transport (Fig. S4E), which suggests that cells growing on digested alginate invest proportionally more of their transcriptome into uptake of not only saccharides but also essential nutrients like iron, zinc, and phosphate, which may become growth-limiting when degradation products are abundantly available.

Both motility and quorum sensing genes increased in expression in cells growing on digested alginate. The positive enrichment of the gene set containing bacterial motility proteins matched the increase in motile cells that we observed in Figure 3E (Fig. 4A, Table S12). The set of quorum sensing genes was also positively enriched in cells growing on digested alginate (Fig. 4A and S4F, Table S13). Quorum sensing is known to control biofilm formation in *Vibrio cholerae*[24,25] and may orchestrate the density-dependent dispersal in the presence of degradation products, though the particular signaling cues remain to be uncovered. The strong cellular response to the degree of alginate depolymerization was also emphasized by the finding that transcription factor genes were enriched among genes with decreased expression on digested alginate (Fig.4, Table S14). The set of genes associated to KEGG's beta-lactam resistance category was enriched in genes with increased expression on digested alginate. However, most genes in this gene set are also associated to the KEGG pathways "Transporters", "Quorum sensing", "Chromosome and associated genes", and "Peptidoglycan biosynthesis" and thus the enrichment likely reflects expression changes in these categories and may relate to the difference in growth dynamics (Fig. 4A and S4G, Table S15). Overall, the observed gene expression changes provide insights into the molecular mechanisms underlying the substantial adaptations of *V. cyclitrophicus* ZF270 cells to the polymeric and digested form of alginate.

bioRxiv preprint doi: https://doi.org/10.1101/2023.07.14.548877; this version posted October 23, 2023. The copyright holder for this preprint (which was not certified by peer review) is the author/funder, who has granted bioRxiv a license to display the preprint in perpetuity. It is made available under aCC-BY-NC-ND 4.0 International license.

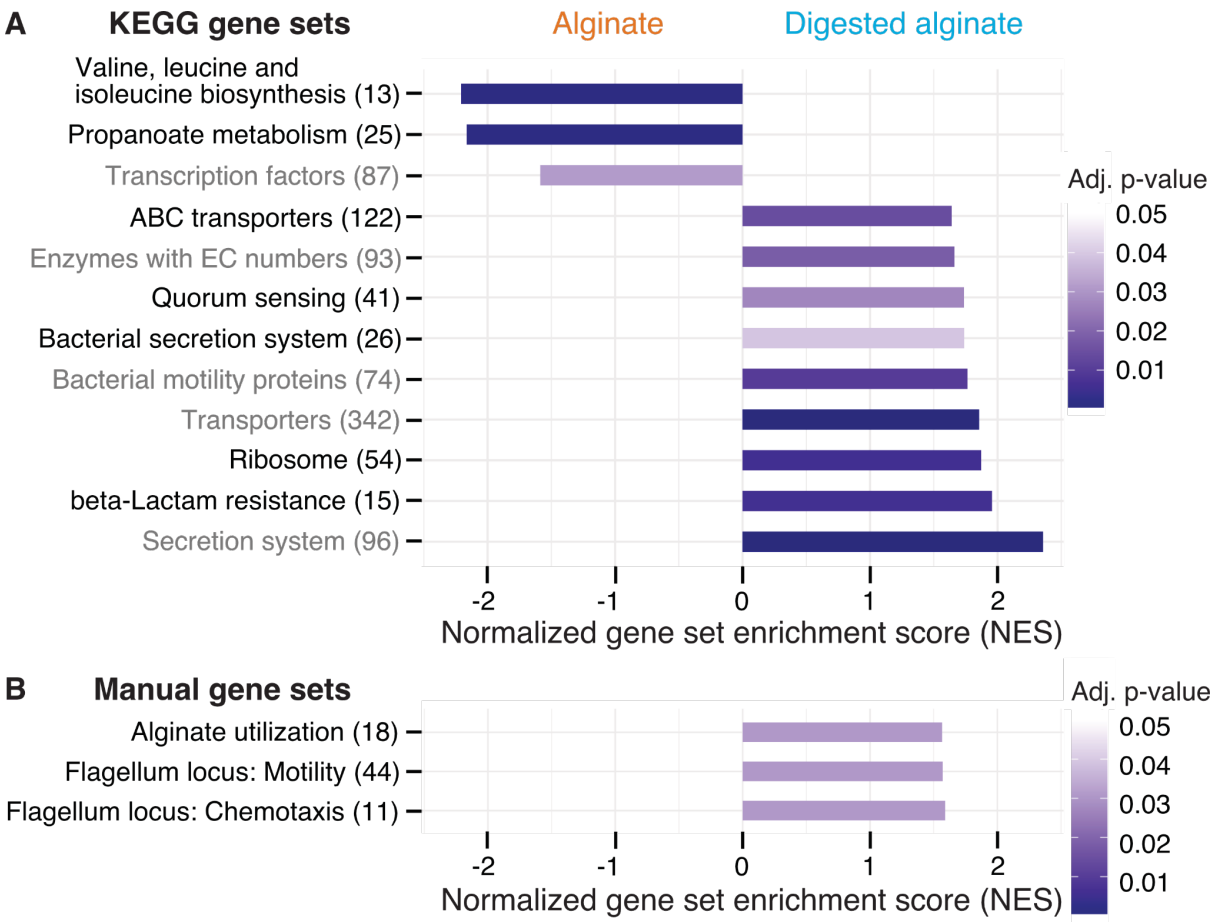

Figure 4. Twelve functional gene sets are enriched in genes with increased or decreased expression in cells grown on digested alginate. Gene set enrichment analysis (GSEA) with (A) all KEGG pathways and KEGG BRITE categories as gene sets or with (B) a custom alginate utilization, flagellar assembly, and flagellum-driven chemotaxis gene set was performed comparing the gene counts of the transcriptome of *V. cyclitrophicus* ZF270 cultures grown on digested alginate and alginate (six replicates each). Gene sets with a positive enrichment score were enriched with genes with higher expression in cells grown on digested alginate relative to cells grown on alginate (BH-adjusted p-value < 0.05), whereas gene sets with negative enrichment scores were significantly enriched with genes with decreased expression on digested alginate. The number in brackets indicates the number of genes with unique K number per gene set (A) and the number of genes per gene set (B) within the *V. cyclitrophicus* ZF270 genome.

Growth on digested alginate is associated with increased expression of alginate catabolism, flagellar motility and chemotaxis genes

For a more fine-grained understanding of the impact of the form of alginate on the alginate catabolism, we investigated specifically the expression of genes involved in alginate degradation, uptake, and

bioRxiv preprint doi: https://doi.org/10.1101/2023.07.14.548877; this version posted October 23, 2023. The copyright holder for this preprint (which was not certified by peer review) is the author/funder, who has granted bioRxiv a license to display the preprint in perpetuity. It is made available under aCC-BY-NC-ND 4.0 International license.

319 catabolism. In the closed genome of *V. cyclitrophicus* ZF270, we identified genes that encode CAZymes
320 responsible for alginate degradation, namely alginate lyase genes from the PL6, PL7, PL15, and PL17
321 family. We identified homologs of alginate transporters (porin *kdgM*, symporter *toaA*, *toaB*, and *toaC*)
322 and metabolic enzymes that shunt into the Entner-Doudoroff pathway (DEHU reductase genes *dehR*,
323 *kdgK*, and *eda*), based on the known genes in the alginate degradation pathway of *Vibrionaceae*[26,27].
324 We found that the expression of most of these genes increased significantly on digested alginate relative
325 to alginate (Fig. 4B, Fig. 5A, S8A, Table S16). Surprisingly, also the expression of most alginate lyase
326 genes increased on digested alginate, especially the expression of secreted alginate lyase genes. This
327 indicates the production of "public" exoenzymes despite the abundance of monomeric and oligomeric
328 degradation products in the digested alginate medium.
329
330 The increased motility of cells observed upon exposure to digested alginate (Fig. 3, Fig. 4A) led us to
331 evaluate the expression of motility- and chemotaxis-associated genes across digested alginate and
332 alginate treatments. As flagella are the main mode of motility in the genus *Vibrio*[28,29], we focused on
333 the expression of flagella-related genes. In the genome of *V. cyclitrophicus* ZF270 we found a gene
334 cluster that encodes most genes involved in flagellar assembly and that was flanked by chemotaxis
335 genes (hereon called flagellar locus, Fig. S8B, and Table S17). Overall, 21/34 flagellar locus genes were
336 differentially expressed (log2 fold change > 0.5, BH-adjusted *p*-value < 0.01) and the majority (90%)
337 of these differentially expressed genes showed increased expression on digested alginate (Fig. 4B). The
338 flagellar genes *flgA*, *fliC*, and *fliH* and the chemotaxis gene *cheW* showed the strongest overexpression
339 (5.4, 3.8, 2.0, and 2.6-fold, respectively). The expression of flagellar biosynthesis genes in *Vibrionacaea*
340 occurs by a cascade of gene expression of four classes of genes (Class I - IV)[30]. We found the expression
341 of the master regulator of the flagellar biosynthesis regulon, the Class I gene *flrA*, to be 1.6-fold
342 increased on digested alginate (BH-adj. *p*-value 3e-19)[31]. The Class II regulatory genes *flrBC*,
343 controlling Class III genes, and *fliA*, controlling Class IV genes, showed 1.5-fold and 1.3-fold increased
344 expression on digested alginate (BH-adj. *p*-value 1e-12 for *flrB*, 2e-39 for *flrC*, 6e-15 for *fliA*) (Fig.
345 5B)[29,32]. These findings suggest that the increased phenotypic motility observed on digested alginate
346 (Fig. 3) is related to the upregulation of flagellar biosynthesis genes. Additionally, the expression of the

bioRxiv preprint doi: https://doi.org/10.1101/2023.07.14.548877; this version posted October 23, 2023. The copyright holder for this preprint (which was not certified by peer review) is the author/funder, who has granted bioRxiv a license to display the preprint in perpetuity. It is made available under aCC-BY-NC-ND 4.0 International license.

flagellum filament, encoded by *fliC* genes of the flagellar locus, was partially increased: *flaD* and *flaC* expression were increased by 3.8 and 1.6-fold, whereas the *flaA* gene was not significantly differentially expressed (BH-adj. *p*-value 7e-37, 2e-19, and 1e-02, respectively) (Fig. 5B, Table S6). This suggests that cells grown on digested alginate have a *flaD*-rich filament composition, which has been shown to alter the swimming and adhesion characteristics of bacterial cells[33,34]. Lastly, we found that most genes involved in chemotaxis and located in the flagellar locus are highly expressed in cells grown on digested alginate (Fig. 5C, Fig. 4B) and likely drive the chemotactic activity of *V. cyclitrophicus* ZF270 during dispersal. Overall, our findings elucidate that cellular responses upon exposure to degradation products manifest in increased expression of genes involved in extracellular alginate breakdown and alginate catabolism as well as flagellar assembly and chemotaxis.

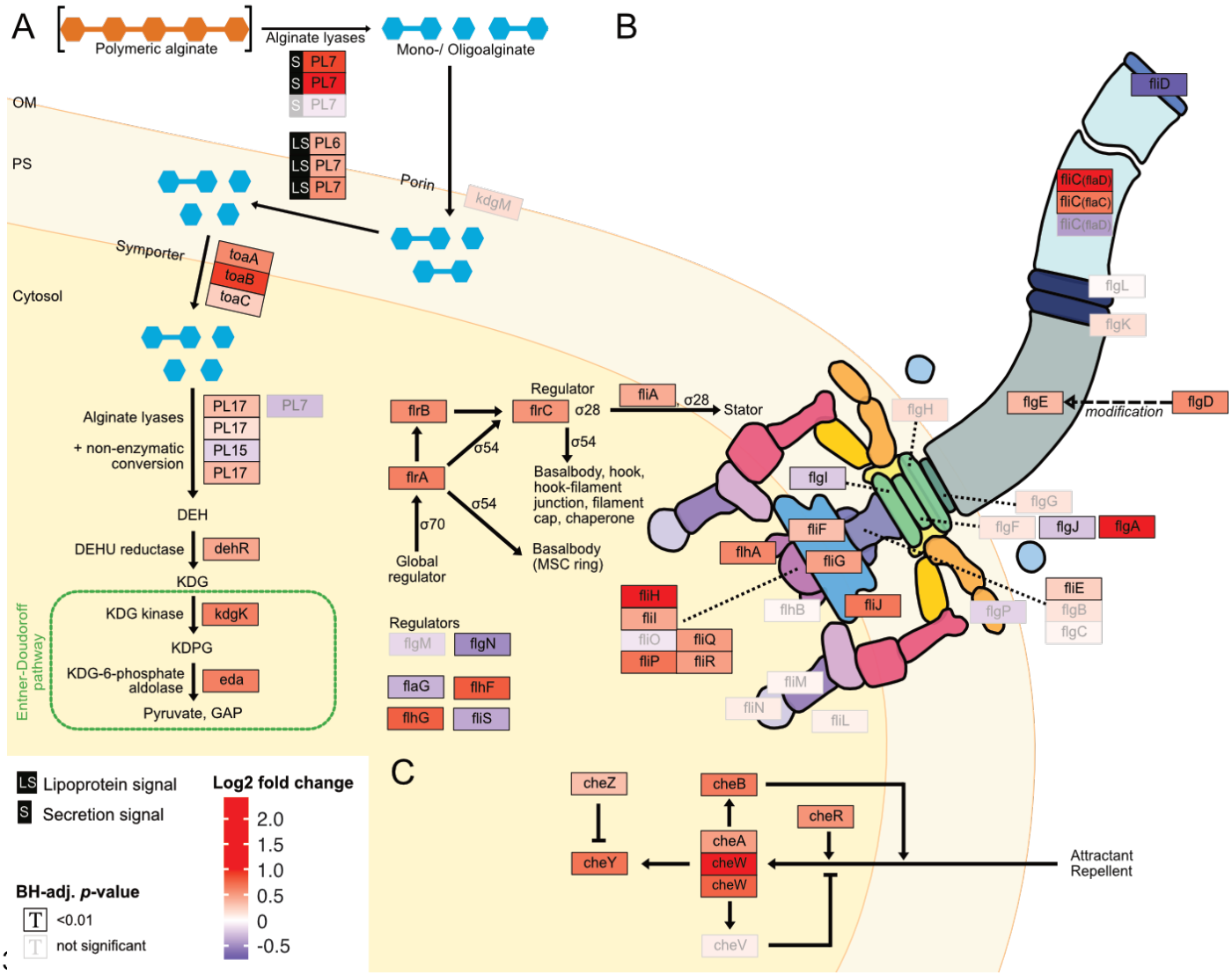

bioRxiv preprint doi: https://doi.org/10.1101/2023.07.14.548877; this version posted October 23, 2023. The copyright holder for this preprint (which was not certified by peer review) is the author/funder, who has granted bioRxiv a license to display the preprint in perpetuity. It is made available under aCC-BY-NC-ND 4.0 International license.

Figure 5. Digested alginate increases expression of genes involved in alginate degradation, uptake and catabolism, as well as flagellar assembly and chemotaxis. Genome-wide differential expression analysis where the log2 fold changes of gene expression on digested alginate compared to alginate is shown for (A) alginate lyases (*PL6, PL7, PL15, PL17*), transporters (porin *kdgM*, symporter *toaB*, symporter *toaC*), and metabolic enzymes shunting into the Entner-Doudoroff pathway (DEHU reductase *DehR*, *kdgK*, *eda*), (B) genes of the flagellar locus associated with flagellar assembly and (C) adjacent chemotaxis genes. Genes displayed in (B) and (C) are part of the KEGG pathways "Bacterial motility proteins" and "Bacterial chemotaxis". Differential expression analysis was performed to compute the Benjamini-Hochberg-adjusted Wald test *p*-value ("BH-adj. *p*-value", text color and box outline color) and log2 fold change (box fill color) for each gene (box). For better visibility, genes that exhibited a log2 fold gene expression change greater than 1 (i.e., doubling of expression) or less than -1 (i.e., halving of expression) are designated maximum intensity of red or blue, respectively. Genes with BH-adj. *p*-value smaller than 0.01 were considered significantly differentially expressed. In (A), the location of the gene products was based on Figure 1 of Wargacki et al.[26] with the exception of the alginate lyases (*PL6*, *PL7*, *PL15*, *PL17*) which were placed based on their signal peptides (S: extracellular, LS: membrane-embedded, none: cytosolic). In (B) and (C) the gene location and depiction were based on the KEGG pathway "Flagellar assembly" (map02040), "Bacterial chemotaxis" (map02030), and Figure 3 of Rajagopala et al.[35]. Genes without known cellular location were omitted here but displayed in the genomic architecture in Fig. S5. Arrow: activation; dashed arrow: modification; "flat" arrow: inhibition; OM: outer membrane; PM: periplasm; IM: inner membrane; PL: polysaccharide lyase family; *kdgM*: oligogalacturonate-specific outer membrane porin; *toaABC*: oligoalginate symporter; DEH: 4-deoxy-L-erythro-5-hexoseulose uronic acid; *dehR*: DEH reductase; KDG: 2-keto-3-deoxy-gluconate; *kdgK*: KDG kinase; KDPG: 2-keto-3-deoxy-6-phosphogluconate; *eda*: KDG-6-phosphate aldolase; GAP: glyceraldehyde 3-phosphate; ED: Entner-Doudoroff; ns: not significant, i.e. BH-adj. *p*-value > 0.01.

Discussion

On Earth organic carbon is mostly present in the form of polysaccharides[1,2], which are often in a particulate state and form a heterogeneous resource landscape. Over the last years, the study of extracellular bacterial degradation of polysaccharides has revealed that bacterial growth on polysaccharides increases with increased cell density, enabling cells to benefit from the exoenzymes and extracellular degradation products of surrounding cells otherwise lost to diffusion ("cooperative

bioRxiv preprint doi: https://doi.org/10.1101/2023.07.14.548877; this version posted October 23, 2023. The copyright holder for this preprint (which was not certified by peer review) is the author/funder, who has granted bioRxiv a license to display the preprint in perpetuity. It is made available under aCC-BY-NC-ND 4.0 International license.

growth")[36–38]. However, cells have been observed not only to aggregate on polysaccharide sources, but also to leave them before the source is depleted[13,38]. This has thus far been interpreted with optimal foraging theory, which weighs the diminishing returns of harvesting resources from a nutrient hotspot against the predation and opportunity costs which ensue[39,40], but the cellular mechanisms that drive the cell dispersal remain unclear.

Our work links these observations and connects them to the cellular mechanisms that underlie the degradation-dispersal cycles of bacterial degraders, which we see as basal drivers of the biogeochemical processing of polysaccharides in heterogeneous nutrient-scapes. When bacteria encounter a new source of biomass, their local environment likely contains few mono- or oligosaccharides but is rich in polysaccharides which usually require extracellular breakdown (Fig. 6, "Finding a new nutrient source"). General concepts of how bacteria recognize the presence of large biopolymers remain elusive, but it was proposed that "sentry" enzymes are constitutively expressed at a basal level to cleave mono- or oligosaccharides from polysaccharides, which cells can take up and which prime their metabolism for the degradation of the respective polysaccharide[41,42]. It is not known yet how widespread the concept of sentry enzymes may be, but the observation of a constitutively expressed PL7 and PL15 family alginate lyase gene in *Z. galactanivorans*[41] is mirrored in our work by the constant expression of an extracellular PL7 family alginate lyase gene, which may act as sentry enzyme that helps to initiate alginate degradation when cells encounter alginate.

It has been previously found that cells grow slowly until a critical cell density for efficient cooperative polymer breakdown is reached[36], observed here as the formation of large cell groups. In this stage, cells start to benefit from the diffusing degradation products and exoenzymes of cells in their local environment and reach their maximal growth rate (Fig. 6, "Early-stage polysaccharide breakdown"). We found that cells grown on degradation products reached their maximal growth earlier and showed increased expression of ribosomal biosynthesis, enzyme secretion, especially of secreted alginate lyases, transporters, quorum sensing and expression changes in the central carbon metabolism. The secretion of secreted alginate lyases might seem surprising and wasteful in a monomer-rich

bioRxiv preprint doi: https://doi.org/10.1101/2023.07.14.548877; this version posted October 23, 2023. The copyright holder for this preprint (which was not certified by peer review) is the author/funder, who has granted bioRxiv a license to display the preprint in perpetuity. It is made available under aCC-BY-NC-ND 4.0 International license.

environment. We speculate that enhanced enzyme secretion supports the continued growth of detached bacteria's offspring that remain on the particle, as observed in the case of *V. splendus* 1AO1 during chitin particle degradation[43]. Another reason may be that cells primarily rely on intracellular monosaccharide levels to trigger the upregulation of genes associated with polysaccharide degradation and catabolism, as seen in *E. coli* across various carbon sources[44,45], unable to modulate the expression of degrading enzymes based on the extracellular presence of monomers.

We show that cells respond to the exposure to degradation products with dispersal from dense cell groups by means of increased flagellum-driven swimming (Fig. 6, "Late-stage polysaccharide breakdown"), decreasing their local cell number. This finding matches with previous observations of cells leaving biopolymer particles before they are depleted[13,38]. A plausible explanation for this density-dependent dispersal is that cells in larger groups compete with each other for nutrients and space, while not profiting from cooperative degradation anymore due to the abundance of degradation products. Motility has also been shown to increase the encounter rate of cells with sources of nutrients[46,47], suggesting motility as a strategy that allows cells to escape from the ensuing competition. Previous work in *Caulobacter crescentus* demonstrated that a flagellum knock-out mutant formed larger cell groups, resulting in reduced growth rates due to intercellular competition[4,14]. While it would be interesting to study non-motile mutants of *V. cyclitrophicus* ZF270, the non-tractability of natural isolates makes direct tests of molecular mechanisms difficult. Additionally, subjecting cells separately to the two monomeric units of alginate or oligomers of defined size could improve our understanding of the specific molecules that trigger motility, but this was experimentally not feasible. We also found that the presence of degradation products increased the expression of chemotaxis genes and detected that cells chemotaxis toward polymeric alginate, but not digested alginate, analogous to previous findings on chitin[46–48]. Even though this may first seem counterintuitive, it makes sense in the light of the dispersal process: chemotaxis towards degradation products would prevent cells from leaving a nutrient source, whereas chemotaxis towards polymers may increase encounters with a fresh nutrient source[49] (Fig. 6, "Finding a new nutrient source"), on which cells can re-initiate degradation. This

bioRxiv preprint doi: https://doi.org/10.1101/2023.07.14.548877; this version posted October 23, 2023. The copyright holder for this preprint (which was not certified by peer review) is the author/funder, who has granted bioRxiv a license to display the preprint in perpetuity. It is made available under aCC-BY-NC-ND 4.0 International license.

strategy allows cells to alternate between degradation and dispersal to acquire carbon and energy in a heterogeneous world with nutrient hotspots[50–53].

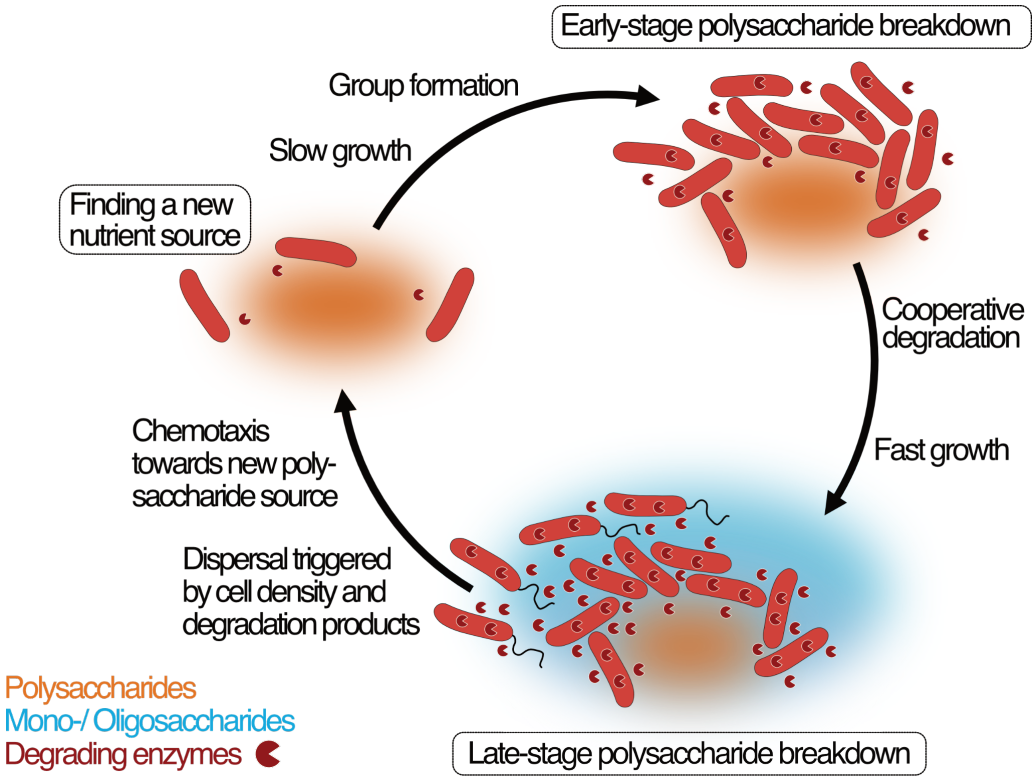

Figure 6. Bacterial growth and regulation on patches of polysaccharides. Based on our findings we propose a conceptual model where degradation of polysaccharides proceeds after the encounter of a polymer source by bacterial cells that have a basal exoenzyme production of "sentry" enzymes ("Encounter of a new carbon source"). This phase is succeeded by group formation, which enables cells to benefit from exoenzymes of neighboring cells and diffusing degradation products ("Early-stage polysaccharide breakdown"). The following phase includes cooperative extracellular degradation of the polysaccharide source, further increasing the concentration of available degradation products. These degradation products trigger the overexpression of alginate degrading, importing, and catabolizing enzymes, ensuring swift polysaccharide degradation ("Late-stage polysaccharide breakdown"). The increased pool of breakdown products also cues flagellar swimming and chemotaxis in a subpopulation of cells towards new polysaccharide sources, thus restarting the cycle of degradation of polymeric carbohydrates by heterotrophic bacteria. Cells and molecules are not drawn to scale. Dark red pie symbols: intracellular and extracellular polysaccharide-degrading enzymes; orange shading: a polymeric carbon source; blue shading: monomeric or oligomeric degradation products.

bioRxiv preprint doi: https://doi.org/10.1101/2023.07.14.548877; this version posted October 23, 2023. The copyright holder for this preprint (which was not certified by peer review) is the author/funder, who has granted bioRxiv a license to display the preprint in perpetuity. It is made available under aCC-BY-NC-ND 4.0 International license.

Conclusion

The heterogeneous landscape of polysaccharide hotspots in natural systems requires bacteria to effectively break down polymeric carbohydrates as well as readily ensure dispersal to new nutrient hotspots. Our findings show that the degree of depolymerization of the polysaccharide influences this decision, altering the growth dynamics, metabolic activity, and motility of cells. Our study also contextualizes the surprising finding that foraging bacteria majorly leave polysaccharide particles before the last third of the particle is consumed[38]. Dispersal from a partially degraded carbon source may serve several purposes: (i) escaping competition that ensues within large cell groups, (ii) ensuring the spread of a part of the clonal population to new environments as bet hedging strategy[40,54], here guided by chemotaxis towards new nutrient hotspots, (iii) preventing whole populations degrading a sinking marine particle or a deposited sediment particle to be buried in depth where nutrient hotspots become sparse[38,55], and/or (iv) increase the genetic variation in bacterial populations[40]. However, dispersal may also occur when a nutrient source offers a surplus of carbon while other essential nutrients become limiting, as the increased expression of iron, zinc, and phosphate transporters in cells grown on digested alginate suggested. These findings emphasize that metabolic molecules can also act as triggers of dispersal, expanding upon the current perspective of dispersal in biofilms as a reaction to dispersal cues like NO, signalling molecules, nutrient starvation, and oxygen starvation[56]. The study of bacterial motility on increasingly complex biomass particles will reveal the role of the nutrient composition of the present nutrient hotspot on the bacterial decision-making. Overall, these new insights into the cellular mechanisms and regulation that drive degradation-dispersal cycles contribute to our understanding of the microbially driven remineralization of biomass, and factors that modulate this process. The open questions of how bacteria sense polysaccharides in their environment, which cell signaling pathways integrate the presence of degradation products in the cellular decision-making of degradation and dispersal, and to what extent cell populations coordinate this decision, present an exciting avenue of further research.

bioRxiv preprint doi: https://doi.org/10.1101/2023.07.14.548877; this version posted October 23, 2023. The copyright holder for this preprint (which was not certified by peer review) is the author/funder, who has granted bioRxiv a license to display the preprint in perpetuity. It is made available under aCC-BY-NC-ND 4.0 International license.

Materials and Methods

Bacterial strains, media and growth assays

Vibrio cyclitrophicus ZF270 (available through Culture Collection Of Switzerland; Accession number: 2043) cells were cultured in Marine Broth (DIFCO) and grown for 18 hours at 25 °C. Cells from these cultures were used for growth experiments in Tibbles Rawling (TR) salts minimal medium[57,58] containing either 0.1% (weight/volume) algae-derived alginate (referred to as "alginate") (Sigma Aldrich, CAS-number 9005-38-3) or 0.1% (weight/volume) digested alginate. The digested alginate was produced by enzymatically digesting 2% alginate with 1 unit ml^{-1} of alginate lyase (Sigma Aldrich, CAS-number 9024-15-1) at 37 °C for 48 hours. Carbon sources were prepared in nanopure water and filter sterilized using 0.40 µm Surfactant-Free Cellulose Acetate filters (Corning, USA). Well-mixed batch experiments in alginate or digested alginate medium were performed in 96-well plates (Greiner Bio) and growth dynamics were measured using a microwell plate reader (Biotek, USA). Assays were initiated as described previously[59]. Briefly, 1 ml from a culture grown for 18 h on Marine broth was centrifuged at 5000 g in 1.5 ml microfuge tubes for 5 minutes. The supernatant was discarded and the cell pellet was subjected to two rounds of washing with the basal TR salts medium. The cell-pellet was then resuspended in 1 ml of TR salts medium and 5 µl of this suspension inoculated into 195 µl TR medium with either carbon source (~10^5 colony forming units (CFUs ml^{-1}) in a 96-well plate (Greiner Bio). The optical density (600 nm) was then measured every 15 minutes for 40 hours. All measurements had six biological replicates.

Alginate oligosaccharide measurements

Oligosaccharide measurements were performed using liquid chromatography time of flight mass spectrometry (LC-QTOF-MS). Samples were prepared by diluting 1:20 in milliQ water and 5 µL of sample was injected per measurement. Chromatographic separation was performed using an Agilent 1290 stack, using an Agilent HILIC-Z column (2.7 µm particles, 2.1 x 50 mm). Mobile phase A contained 10% acetonitrile (Fisher Scientific) and 0.1% medronic acid (Agilent), and Mobile phase B contained 90% acetonitrile and 0.1% medronic acid. The separation was performed as follows: Mobile phase B 100% for 1 minute, gradient to 30% phase B over 3 minutes, 30% phase B for 30 seconds, and

bioRxiv preprint doi: https://doi.org/10.1101/2023.07.14.548877; this version posted October 23, 2023. The copyright holder for this preprint (which was not certified by peer review) is the author/funder, who has granted bioRxiv a license to display the preprint in perpetuity. It is made available under aCC-BY-NC-ND 4.0 International license.

equilibration of 100% phase B for 5 minutes. The flow rate was 400 µL min^{-1} at 30 °C. Samples were measured using an Agilent 6520 mass spectrometer in negative mode, in 4 GHz high-resolution mode. Data analysis was performed in Agilent Quantitative Analysis software.

Microfluidics and time-lapse microscopy

Microfluidic experiments and microscopy were performed as described previously[14,16,60]. Cells were imaged within chambers of a PDMS (Sylgard-Dow) microfluidic chip that ranged in size from 60-120 × 60 × 0.56 µm ($l \times b \times h$). Within these chambers, cells can attach to the glass surface and experience the medium that diffuses through lateral flow channels. Imaging was performed using IX83 inverted microscope systems (Olympus, Japan) with automated stage controller (Marzhauser Wetzlar, Germany), shutter, and laser-based autofocus system (Olympus ZDC 2). Chambers were imaged in parallel on the same PDMS chip, and phase-contrast images of each position were taken every 8 or 10 minutes. The microscopy unit and PDMS chip were maintained at 25 °C using a cellVivo microscope incubation system (Pecon GmbH).

Motility assays

Cells were grown for 10 hours in Marine Broth (DIFCO) after which 10 µl of culture was used to inoculate culture tubes (Greiner) containing 5 ml of TR medium with either 0.1% alginate or 0.1% digested alginate. After 6 hours of growth at 25 °C, 2 µl of cell suspension was inoculated into microfluidic growth chambers. Cells within six replicate chambers were then imaged with the phase-contrast channel at a high frame rate (125 Hz, i.e., frames s^{-1}) using the same microscopy setup described above.

Chemotaxis assays

To assess whether polymeric alginate and digested alginate attract *Vibrio cyclitrophicus* ZF270, we used the *In Situ* Chemotaxis Assay[17,18] (ISCA), a microfluidic device consisting of a 5 × 5 array of microwells that can be individually loaded with solutions of different chemicals (110 µl each). Once the ISCA is deployed in an aqueous environment, the chemicals diffuse out of the wells through a small

bioRxiv preprint doi: https://doi.org/10.1101/2023.07.14.548877; this version posted October 23, 2023. The copyright holder for this preprint (which was not certified by peer review) is the author/funder, who has granted bioRxiv a license to display the preprint in perpetuity. It is made available under aCC-BY-NC-ND 4.0 International license.

port, creating chemical gradients which will guide chemotactic bacteria inside the wells of the device[17,18]. *Vibrio cyclitrophicus* ZF210 was plated on Marine Agar (BD Difco) from a glycerol stock and grown for 16 h at 27 °C. A single colony was then incubated in 10% Marine Broth (BD Difco) in 0.22-µm filtered artificial seawater (Instant Ocean, Spectrum Brands) and grown overnight at 27 °C and 180 rpm. The culture was diluted down to 1 x 10^6 cells ml^{-1} in 0.22 µm filtered artificial seawater (Instant Ocean, Spectrum Brands) to perform the chemotaxis experiment. Both chemoattractants (alginate and digested alginate) were diluted in sterile seawater (35 g l^{-1}; Instant Ocean, Spectrum Brands) at a final concentration of 0.1% and then filtered with a 0.2 µm filter (Millipore) to remove particles and potential contaminants. Within the ISCA, one full row of five wells was used per chemoattractant as technical replicates. The chemoattractants were injected in triplicate ISCA with a sterile 1 ml syringe (Codau) and needle (27 G, Henke Sass Wolf). A last row containing 0.2 µm-filtered seawater acted as negative control accounting for cells swimming in the device by random motility only. Experiments were conducted by incubating the ISCAs for 1 h in the diluted *Vibrio cyclitrophicus* ZF270 culture. Upon time completion, a sterile syringe and needle were used to retrieve the content of the wells and transferred to 1 ml microfuge tubes resulting in a pooling of a row of 5 wells containing the same sample. Sample staining was performed with SYBR Green I (Thermo Fisher) and the chemotactic response was quantified by counting cells using flow cytometry. The strength of the chemotactic response was determined by the mean chemotactic index (I_C), defined as the ratio of the number of cells found in each chemoattractant to the number of cells in control wells containing filtered seawater (so that attraction corresponds to $I_C > 1$).

Culturing and harvesting cells for transcriptomics

Cells were grown for 18 hours in Marine Broth (DIFCO) after which 1 ml of culture was centrifuged at 5000 g in 1.5 ml microfuge tubes for 5 minutes. The supernatant was discarded and the cell pellet was subjected to two rounds of washing with the basal TR salts medium. The cell pellet was then resuspended in 1 ml of TR salts medium and 250 µl of this suspension were used to inoculate 100 ml flasks (Schott-Duran) containing 10 ml of TR medium with either 0.1% alginate or 0.1% digested alginate. This was done in parallel for six flasks. Once cultures in the flasks reached mid-exponential

bioRxiv preprint doi: https://doi.org/10.1101/2023.07.14.548877; this version posted October 23, 2023. The copyright holder for this preprint (which was not certified by peer review) is the author/funder, who has granted bioRxiv a license to display the preprint in perpetuity. It is made available under aCC-BY-NC-ND 4.0 International license.

phase (10 hours and 15 hours after inoculation for digested alginate and alginate, respectively) and had approximately the same OD (0.39 for digested alginate and 0.41 for alginate), 2 ml of cultures were harvested for RNA extraction. Samples were stabilized with the RNprotect reagent (Qiagen) and RNA was extracted using the RNeasy mini kit (Qiagen).

Sequencing and gene annotation of Vibrio cyclitrophicus ZF270

Long read sequencing using the Oxford Nanopore Platform (Long read DNA sequencing kit) and short read sequencing using the Illumina platform (Illumina DNA Prep kit and IDT 10bp UDI indices, and sequenced on an Illumina NextSeq 2000 producing 2x151bp reads) was performed by the Microbial Genome Sequencing Center, Pittsburgh, USA (MiGS), to create a new closed reference genome of *V. cyclitrophicus* ZF270 (BioProject PRJNA991487). Annotation of this genome was done with RASTtk (v2.0, Rapid Annotation using Subsystem Technology tool kit[61]). Additionally, KEGG Ontology identifiers ("K numbers") were annotated with BlastKOALA (v2.2)[62]. Dedicated annotation of alginate lyase genes was performed by homology search for proteins belonging to the PL5, PL6, PL7, PL14, PL15, PL17, PL18, PL31, PL36, or PL39 family[63] by dbCAN2 (v9.0)[64]. Enzymes for alginate transport and metabolism were identified by BLASTn-search[65,66] of gene sequences of *Vibrio splendidus* 12B01, which were previously identified as minimum genetic prerequisites for alginate utilization and enabled alginate degradation when cloned into *E. coli*[26].

Location prediction of alginate lyases

Signal peptides were annotated using SignalP (v.5.0)[67], and LipoP (v.1.0)[68]. SignalP discriminated between 1) Sec/SPI: "standard" secretory signal peptides transported by the Sec translocon and cleaved by Signal Peptidase I (SPI), 2) Sec/SPII: lipoprotein signal peptides transported by the Sec translocon and cleaved by Signal Peptidase II (SPII), and 3) Tat/SPI: Tat signal peptides transported by the Tat translocon and cleaved by SPI. LipoP discriminates between 1) SPI: signal peptide, 2) SpII: lipoprotein signal peptide, and 3) TMH: n-terminal transmembrane helix. All predictions were in agreement, apart from one PL7 (gene 1136176.5.peg.4375) which was predicted by LipoP as cytoplasmic and by SignalP as equally likely cytoplasmic as containing a lipoprotein signal peptide.

bioRxiv preprint doi: https://doi.org/10.1101/2023.07.14.548877; this version posted October 23, 2023. The copyright holder for this preprint (which was not certified by peer review) is the author/funder, who has granted bioRxiv a license to display the preprint in perpetuity. It is made available under aCC-BY-NC-ND 4.0 International license.

Transcriptomic analysis: Sequencing, pre-processing, differential expression analysis, and functional analysis

Sequencing (12 M reads, 2 x 50 bp) of the isolated RNA was performed by MiGS after rRNA depletion using RiboZero Plus (Ilumina). cDNA libraries were prepared using an Illumina DNA Prep kit and IDT 10 bp UDI indices, and sequenced on an Illumina NextSeq 2000. Preprocessing of the raw reads was carried out as follows: Quality control was performed with FastQC (v0.11.9)[69] and reads were trimmed with Trimmomatic (v0.38)[70]; the high-quality reads were mapped to the reference genome (described above) with Bowtie2 (v2.3.5.1)[71]; binarization, sorting, and indexing were done with Samtools (v1.10)[72]; gene counts were computed with the featureCount function of Subread (v2.0.1)[73].

Differential expression analysis was performed with DESeq2 (v1.30.1)[74]. In brief, DESeq2 normalizes the raw read counts with normalization factors ("size factors") to account for differences in sequencing depth between samples. Subsequently, gene-wise dispersion estimates are computed for each gene separately using maximum likelihood, and then shrunk toward the values predicted by the dispersion-mean dependence curve to obtain final dispersion values. Finally, DESeq2 fits a negative binomial model to the read counts and performs significance testing using the Wald test. Here reported *p*-values result from the Wald test of read counts from the digested alginate condition compared to the alginate condition and were adjusted for multiple testing by Benjamini-Hochberg correction[75] as implemented in the p.adjust function of base R (v4.1.2). The reported log2 fold changes indicate the log2(DESeq2-normalised reads in digested alginate condition / DESeq2-normalised reads in alginate condition) for each gene.

Visualization of gene maps was performed in R with the ggplot2 package (v3.4.0) and the extension gggenes (v0.4.1) by David Wilkins.

For systematic functional analysis we performed gene set enrichment analysis (GSEA)[19] using the fgsea function of the fgsea package (v1.20.0) with minimal number of unique genes per gene set "minSize" = 5 and number of permutations "nPermSimple" = 1000000. In brief, GSEA takes the full gene list ranked by log2 fold change and annotated with K numbers as input and determines whether the member genes of any KEGG pathway are randomly distributed throughout the ranked gene list or whether they

bioRxiv preprint doi: https://doi.org/10.1101/2023.07.14.548877; this version posted October 23, 2023. The copyright holder for this preprint (which was not certified by peer review) is the author/funder, who has granted bioRxiv a license to display the preprint in perpetuity. It is made available under aCC-BY-NC-ND 4.0 International license.

are primarily found at the top or bottom[19]. This is quantified by the enrichment score (ES), which corresponds to a weighted Kolmogorov-Smirnov-like statistic. The ES of each gene set is normalized to the mean enrichment of random samples of the same size to account for the size of the set, yielding the normalized enrichment score (NES). To estimate the significance level of the enrichment score, the *p*-value of the observed enrichment score is calculated relative to a null distribution that was computed from permuted data. The estimated significance level was adjusted to account for multiple hypothesis testing. As gene sets we chose all KEGG pathways and KEGG BRITE categories (as noted in Table S1 in column "KEGG_pathway") within all genes of *V. cyclitrophicus* ZF270 annotated with a KEGG Ontology identifier ("K number"). Visualization of differential expression levels in KEGG pathways was performed with the R package pathview (v1.35.0)[76]. We also formed gene sets of the genes associated with alginate utilization (see "*Sequencing and gene annotation of Vibrio cyclitrophicus* ZF270", Table S16), of the genes of the flagellar locus that map to the KEGG pathways "Bacterial motility proteins", and of the genes of the flagellar locus that map to the KEGG pathways "Bacterial chemotaxis" (as noted in Table S17) within all genes of *V. cyclitrophicus* ZF270.

Image analysis

Cells within microscopy images were segmented and tracked using ilastik (v1.3) ("pixel classification workflow" and "tracking with probabilities workflow"). Phase contrast images were used for alignment, segmentation, tracking and linking. Images were cropped at the boundaries of each microfluidic chamber. The lineage identity of each single cell was assigned by ilastik's tracking plugin and visualized by coloring the segmented cells, respectively. The growth rate of each cell was computed as the change of cell area over time, i.e., via a linear regression of the single-cell area over the time between consecutive cell divisions, based on ilastik's segmentation and tracking output. Cells that were tracked over less than three frames were excluded. Measurement of swimming speeds and displacement of cells was performed using ilastik (v1.4), ImageJ (v2.3) and Trackmate (v7.5.2). Briefly, cell-segmentation ("pixel classification workflow" in ilastik) and tracking ("animal tracking workflow" in ilastik) were performed using the high frame rate phase contrast images in ilastik (v1.4). Cell trajectories and properties were then computed using the output of the ilastik workflow in Trackmate.

bioRxiv preprint doi: https://doi.org/10.1101/2023.07.14.548877; this version posted October 23, 2023. The copyright holder for this preprint (which was not certified by peer review) is the author/funder, who has granted bioRxiv a license to display the preprint in perpetuity. It is made available under aCC-BY-NC-ND 4.0 International license.

655

656 *Dispersal analysis*

657 For the analysis on the dispersal of cells (Fig. 2), we computed the cell number as the total number of
658 cells within a microfluidic chamber. The change in the number of cells was computed by subtracting
659 the number of cells before the medium switch (i.e., average number of cells between t = 1.9 to 2.1 h)
660 from the number of cells after the medium switch (i.e., average number of cells between t = 3.9 to 5.5
661 h).

662

663 *Datasets and statistical analysis*

664 All batch experiments were replicated 3 to 6 times. Growth curves were analyzed in Python (v3.7) using
665 the *Amiga* package (v1.1.0)[77] and GraphPad Prism (v8, GraphPad Software). The microscopy dataset
666 consisted of eight chambers each, corresponding to the eight replicates shown in Figure 1 and Figure 2.
667 These were grouped into two biological replicates wherein each biological replicate was fed by media
668 through a unique channel in a microfluidic chip. Cells with negative growth rates were excluded from
669 the analysis after visual curation, as they represented artefacts, mistakes in segmentation or linking
670 during the tracking process, or non-growing deformed cells. Each chamber was treated as an
671 independent replicate. Comparisons were considered statistically significant when $p < 0.05$ or when the
672 False Discovery Rate (FDR)-corrected q was smaller than 0.05. FDR corrections were applied when
673 multiple t tests were performed for the same dataset. Measures of effect size are represented by the R^2
674 or eta^2 value. All statistical analyses were performed in GraphPad Prism v9.0 (GraphPad Software,
675 USA), R v4.1.2, RStudio v1.1.463 (Posit, USA).

676

677 **Acknowledgements:** We thank past and present members of the Microbial Systems Ecology group for
678 feedback. This research was supported by an ETH fellowship and a Marie Skłodowska-Curie Actions
679 for People COFUND program fellowship (FEL-37-16-1) to GD; an ETH Career Seed Grant to GD
680 (FEL-14 18-1), the Simons Foundation Collaboration on Principles of Microbial Ecosystems (PriME,
681 #542379 and #542395) to MA and RS; and by ETH Zurich and Eawag.

682

bioRxiv preprint doi: https://doi.org/10.1101/2023.07.14.548877; this version posted October 23, 2023. The copyright holder for this preprint (which was not certified by peer review) is the author/funder, who has granted bioRxiv a license to display the preprint in perpetuity. It is made available under aCC-BY-NC-ND 4.0 International license.

Data Availability: Sequencing data is available on NCBI, BioProject PRJNA991487, upon publication. All further data is deposited on ERIC Open (https://opendata.eawag.ch/, https://doi.org/10.25678/0008MH), available upon publication. All code will be made publicly accessible on https://github.com/Microbial-Systems-Ecology/publications upon publication.

Competing interests: The authors declare no competing interests.

Author Contributions: GD, AS, JS, and JK conceived the research along with MA. GD designed and performed the experiments. AS developed and implemented the algorithms to compute single-cell growth rates and visualize lineage identities from segmented and tracked cells. AS analyzed and visualized the RNA-seq data. JK conceived and implemented the cell dispersal analysis. EC conducted the ISCA experiment. SP carried out the mass spectrometry measurements. AS and GD analyzed the data with inputs from JK, JS, CM, MA, and RS. AS wrote the manuscript with inputs from GD, OS, MA, JK, JS, EC, SP, CM, and RS.

Citations:

1. BeMiller JN. 4 - Polysaccharides: Occurrence, Structures, and Chemistry. In: BeMiller JN, ed. *Carbohydrate Chemistry for Food Scientists (Third Edition)*. AACC International Press; 2019:75-101. doi:10.1016/B978-0-12-812069-9.00004-2

2. Reintjes G, Arnosti C, Fuchs B, Amann R. Selfish, sharing and scavenging bacteria in the Atlantic Ocean: a biogeographical study of bacterial substrate utilisation. *ISME J*. 2019;13(5):1119-1132. doi:10.1038/s41396-018-0326-3

3. Ratzke C, Gore J. Self-organized patchiness facilitates survival in a cooperatively growing Bacillus subtilis population. *Nature Microbiology*. 2016;1(5):16022. doi:10.1038/nmicrobiol.2016.22

4. Povolo VR, D'Souza GG, Kaczmarczyk A, Stubbusch AK, Jenal U, Ackermann M. Extracellular appendages govern spatial dynamics and growth of Caulobacter crescentus on a prevalent biopolymer. *bioRxiv*. Published online January 1, 2022:2022.06.13.495907. doi:10.1101/2022.06.13.495907

5. Westrich JR, Griffin DW, Westphal DL, Lipp EK. Vibrio Population Dynamics in Mid-Atlantic Surface Waters during Saharan Dust Events. *Frontiers in Marine Science*. 2018;5. https://www.frontiersin.org/articles/10.3389/fmars.2018.00012

bioRxiv preprint doi: https://doi.org/10.1101/2023.07.14.548877; this version posted October 23, 2023. The copyright holder for this preprint (which was not certified by peer review) is the author/funder, who has granted bioRxiv a license to display the preprint in perpetuity. It is made available under aCC-BY-NC-ND 4.0 International license.

6. Takemura A, Chien D, Polz M. Associations and dynamics of Vibrionaceae in the environment, from the genus to the population level. *Frontiers in Microbiology*. 2014;5. https://www.frontiersin.org/articles/10.3389/fmicb.2014.00038

7. Schwartzman JA, Ebrahimi A, Chadwick G, Sato Y, Orphan V, Cordero OX. Bacterial growth in multicellular aggregates leads to the emergence of complex lifecycles. *bioRxiv*. Published online January 1, 2021:2021.11.01.466752. doi:10.1101/2021.11.01.466752

8. D'Souza G, Ebrahimi A, Stubbusch A, et al. Cell aggregation is associated with enzyme secretion strategies in marine polysaccharide-degrading bacteria. *ISME J*. Published online February 22, 2023. doi:10.1038/s41396-023-01385-1

9. Wang X, Liu J, Liang J, Sun H, Zhang XH. Spatiotemporal dynamics of the total and active Vibrio spp. populations throughout the Changjiang estuary in China. *Environmental Microbiology*. 2020;22(10):4438-4455. doi:10.1111/1462-2920.15152

10. Mabeau S, Kloareg B. Isolation and Analysis of the Cell Walls of Brown Algae: Fucus spiralis, F. ceranoides, F. vesiculosus, F. serratus, Bifurcaria bifurcata and Laminaria digitata. *Journal of Experimental Botany*. 1987;38(9):1573-1580. doi:10.1093/jxb/38.9.1573

11. Wong TY, Preston LA, Schiller NL. Alginate Lyase: Review of Major Sources and Enzyme Characteristics, Structure-Function Analysis, Biological Roles, and Applications. *Annual Review of Microbiology*. 2000;54(1):289-340. doi:10.1146/annurev.micro.54.1.289

12. Hunt DE, David LA, Gevers D, Preheim SP, Alm EJ, Polz MF. Resource Partitioning and Sympatric Differentiation Among Closely Related Bacterioplankton. *Science*. Published online May 23, 2008. doi:10.1126/science.1157890

13. Yawata Y, Cordero OX, Menolascina F, Hehemann JH, Polz MF, Stocker R. Competition–dispersal tradeoff ecologically differentiates recently speciated marine bacterioplankton populations. *Proc Natl Acad Sci USA*. 2014;111(15):5622-5627. doi:10.1073/pnas.1318943111

14. D'Souza GG, Povolo VR, Keegstra JM, Stocker R, Ackermann M. Nutrient complexity triggers transitions between solitary and colonial growth in bacterial populations. *ISME J*. 2021;15(9):2614-2626. doi:10.1038/s41396-021-00953-7

15. Huang L, Zhou J, Li X, Peng Q, Lu H, Du Y. Characterization of a new alginate lyase from newly isolated *Flavobacterium* sp. S20. *Journal of Industrial Microbiology and Biotechnology*. 2013;40(1):113-122. doi:10.1007/s10295-012-1210-1

16. Dal Co A, van Vliet S, Kiviet DJ, Schlegel S, Ackermann M. Short-range interactions govern the dynamics and functions of microbial communities. *Nat Ecol Evol*. 2020;4(3):366-375. doi:10.1038/s41559-019-1080-2

17. Lambert BS, Raina JB, Fernandez VI, et al. A microfluidics-based in situ chemotaxis assay to study the behaviour of aquatic microbial communities. *Nat Microbiol*. 2017;2(10):1344-1349. doi:10.1038/s41564-017-0010-9

18. Clerc EE, Raina JB, Lambert BS, Seymour J, Stocker R. In Situ Chemotaxis Assay to Examine Microbial Behavior in Aquatic Ecosystems. *JoVE*. 2020;(159):e61062. doi:10.3791/61062

19. Subramanian A, Tamayo P, Mootha VK, et al. Gene set enrichment analysis: a knowledge-based approach for interpreting genome-wide expression profiles. *Proc Natl Acad Sci U S A*. 2005;102(43):15545-15550. doi:10.1073/pnas.0506580102

bioRxiv preprint doi: https://doi.org/10.1101/2023.07.14.548877; this version posted October 23, 2023. The copyright holder for this preprint (which was not certified by peer review) is the author/funder, who has granted bioRxiv a license to display the preprint in perpetuity. It is made available under aCC-BY-NC-ND 4.0 International license.

20. Wei Y, Lee JM, Richmond C, Blattner FR, Rafalski JA, LaRossa RA. High-Density Microarray-Mediated Gene Expression Profiling of *Escherichia coli*. *J Bacteriol*. 2001;183(2):545-556. doi:10.1128/JB.183.2.545-556.2001

21. Gifford SM, Sharma S, Booth M, Moran MA. Expression patterns reveal niche diversification in a marine microbial assemblage. *ISME J*. 2013;7(2):281-298. doi:10.1038/ismej.2012.96

22. Johnson TL, Fong JC, Rule C, Rogers A, Yildiz FH, Sandkvist M. The Type II Secretion System Delivers Matrix Proteins for Biofilm Formation by Vibrio cholerae. *J Bacteriol*. 2014;196(24):4245-4252. doi:10.1128/JB.01944-14

23. Sikora AE. Proteins Secreted via the Type II Secretion System: Smart Strategies of Vibrio cholerae to Maintain Fitness in Different Ecological Niches. Heitman J, ed. *PLoS Pathog*. 2013;9(2):e1003126. doi:10.1371/journal.ppat.1003126

24. Jemielita M, Wingreen NS, Bassler BL. Quorum sensing controls Vibrio cholerae multicellular aggregate formation. Storz G, ed. *eLife*. 2018;7:e42057. doi:10.7554/eLife.42057

25. Waters CM, Lu W, Rabinowitz JD, Bassler BL. Quorum sensing controls biofilm formation in Vibrio cholerae through modulation of cyclic di-GMP levels and repression of vpsT. *J Bacteriol*. 2008;190(7):2527-2536. doi:10.1128/JB.01756-07

26. Wargacki AJ, Leonard E, Win MN, et al. An Engineered Microbial Platform for Direct Biofuel Production from Brown Macroalgae. *Science*. Published online January 20, 2012. doi:10.1126/science.1214547

27. Zhang L, Li X, Zhang X, Li Y, Wang L. Bacterial alginate metabolism: an important pathway for bioconversion of brown algae. *Biotechnol Biofuels*. 2021;14(1):158. doi:10.1186/s13068-021-02007-8

28. Khan F, Tabassum N, Anand R, Kim YM. Motility of Vibrio spp.: regulation and controlling strategies. *Appl Microbiol Biotechnol*. 2020;104(19):8187-8208. doi:10.1007/s00253-020-10794-7

29. Echazarreta MA, Klose KE. Vibrio Flagellar Synthesis. *Front Cell Infect Microbiol*. 2019;9:131. doi:10.3389/fcimb.2019.00131

30. Prouty MG, Correa NE, Klose KE. The novel sigma54- and sigma28-dependent flagellar gene transcription hierarchy of Vibrio cholerae. *Mol Microbiol*. 2001;39(6):1595-1609. doi:10.1046/j.1365-2958.2001.02348.x

31. Klose KE, Mekalanos JJ. Differential Regulation of Multiple Flagellins in *Vibrio cholerae*. *J Bacteriol*. 1998;180(2):303-316. doi:10.1128/JB.180.2.303-316.1998

32. Srivastava D, Hsieh ML, Khataokar A, Neiditch MB, Waters CM. Cyclic di-GMP inhibits Vibrio cholerae motility by repressing induction of transcription and inducing extracellular polysaccharide production. *Mol Microbiol*. 2013;90(6):1262-1276. doi:10.1111/mmi.12432

33. Kim SY, Thanh XTT, Jeong K, et al. Contribution of six flagellin genes to the flagellum biogenesis of Vibrio vulnificus and in vivo invasion. *Infect Immun*. 2014;82(1):29-42. doi:10.1128/iai.00654-13

34. Nedeljković M, Sastre DE, Sundberg EJ. Bacterial Flagellar Filament: A Supramolecular Multifunctional Nanostructure. *Int J Mol Sci*. 2021;22(14):7521. doi:10.3390/ijms22147521

bioRxiv preprint doi: https://doi.org/10.1101/2023.07.14.548877; this version posted October 23, 2023. The copyright holder for this preprint (which was not certified by peer review) is the author/funder, who has granted bioRxiv a license to display the preprint in perpetuity. It is made available under aCC-BY-NC-ND 4.0 International license.

35. Rajagopala SV, Titz B, Goll J, et al. The protein network of bacterial motility. *Mol Syst Biol*. 2007;3(1):128. doi:10.1038/msb4100166

36. Ebrahimi A, Schwartzman J, Cordero OX. Cooperation and spatial self-organization determine rate and efficiency of particulate organic matter degradation in marine bacteria. *Proc Natl Acad Sci USA*. 2019;116(46):23309-23316. doi:10.1073/pnas.1908512116

37. Drescher K, Nadell CD, Stone HA, Wingreen NS, Bassler BL. Solutions to the Public Goods Dilemma in Bacterial Biofilms. *Current Biology*. 2014;24(1):50-55. doi:10.1016/j.cub.2013.10.030

38. Alcolombri U, Peaudecerf FJ, Fernandez VI, Behrendt L, Lee KS, Stocker R. Sinking enhances the degradation of organic particles by marine bacteria. *Nat Geosci*. 2021;14(10):775-780. doi:10.1038/s41561-021-00817-x

39. Yawata Y, Carrara F, Menolascina F, Stocker R. Constrained optimal foraging by marine bacterioplankton on particulate organic matter. *Proc Natl Acad Sci USA*. 2020;117(41):25571-25579. doi:10.1073/pnas.2012443117

40. McDougald D, Rice SA, Barraud N, Steinberg PD, Kjelleberg S. Should we stay or should we go: mechanisms and ecological consequences for biofilm dispersal. *Nat Rev Microbiol*. 2012;10(1):39-50. doi:10.1038/nrmicro2695

41. Thomas F, Barbeyron T, Tonon T, Génicot S, Czjzek M, Michel G. Characterization of the first alginolytic operons in a marine bacterium: from their emergence in marine Flavobacteriia to their independent transfers to marine Proteobacteria and human gut Bacteroides: Emergence and transfer of alginolytic operons. *Environmental Microbiology*. 2012;14(9):2379-2394. doi:10.1111/j.1462-2920.2012.02751.x

42. Dudek M, Dieudonné A, Jouanneau D, et al. Regulation of alginate catabolism involves a GntR family repressor in the marine flavobacterium Zobellia galactanivorans DsijT. *Nucleic Acids Research*. 2020;48(14):7786-7800. doi:10.1093/nar/gkaa533

43. Guessous G, Patsalo V, Balakrishnan R, Çağlar T, Williamson JR, Hwa T. Inherited chitinases enable sustained growth and rapid dispersal of bacteria from chitin particles. *Nat Microbiol*. 2023;8(9):1695-1705. doi:10.1038/s41564-023-01444-5

44. Chubukov V, Gerosa L, Kochanowski K, Sauer U. Coordination of microbial metabolism. *Nat Rev Microbiol*. 2014;12(5):327-340. doi:10.1038/nrmicro3238

45. Martínez-Antonio A, Janga SC, Salgado H, Collado-Vides J. Internal-sensing machinery directs the activity of the regulatory network in Escherichia coli. *Trends in Microbiology*. 2006;14(1):22-27. doi:10.1016/j.tim.2005.11.002

46. Bassler BL, Gibbons PJ, Yu C, Roseman S. Chitin utilization by marine bacteria. Chemotaxis to chitin oligosaccharides by Vibrio furnissii. *Journal of Biological Chemistry*. 1991;266(36):24268-24275. doi:10.1016/S0021-9258(18)54224-1

47. Meibom KL, Li XB, Nielsen AT, Wu CY, Roseman S, Schoolnik GK. The *Vibrio cholerae* chitin utilization program. *Proc Natl Acad Sci USA*. 2004;101(8):2524-2529. doi:10.1073/pnas.0308707101

48. Mandel MJ, Schaefer AL, Brennan CA, et al. Squid-Derived Chitin Oligosaccharides Are a Chemotactic Signal during Colonization by Vibrio fischeri. *Appl Environ Microbiol*. 2012;78(13):4620-4626. doi:10.1128/AEM.00377-12

bioRxiv preprint doi: https://doi.org/10.1101/2023.07.14.548877; this version posted October 23, 2023. The copyright holder for this preprint (which was not certified by peer review) is the author/funder, who has granted bioRxiv a license to display the preprint in perpetuity. It is made available under aCC-BY-NC-ND 4.0 International license.

49. Purcell EM. Life at low Reynolds number. *American Journal of Physics*. 1977;45(1):3-11. doi:10.1119/1.10903

50. Blackburn N, Fenchel T, Mitchell J. Microscale Nutrient Patches in Planktonic Habitats Shown by Chemotactic Bacteria. *Science*. 1998;282(5397):2254-2256. doi:10.1126/science.282.5397.2254

51. Blackburn N, Fenchel T. Influence of bacteria, diffusion and shear on micro-scale nutrient patches, and implications for bacterial chemotaxis. *Mar Ecol Prog Ser*. 1999;189:1-7. doi:10.3354/meps189001

52. Fenchel T. Microbial Behavior in a Heterogeneous World. *Science*. 2002;296(5570):1068-1071. doi:10.1126/science.1070118

53. Smriga S, Fernandez VI, Mitchell JG, Stocker R. Chemotaxis toward phytoplankton drives organic matter partitioning among marine bacteria. *Proc Natl Acad Sci USA*. 2016;113(6):1576-1581. doi:10.1073/pnas.1512307113

54. Ronce O. How Does It Feel to Be Like a Rolling Stone? Ten Questions About Dispersal Evolution. *Annu Rev Ecol Evol Syst*. 2007;38(1):231-253. doi:10.1146/annurev.ecolsys.38.091206.095611

55. Fenchel T. Motility of bacteria in sediments. *Aquat Microb Ecol*. 2008;51:23-30. doi:10.3354/ame01182

56. Rumbaugh KP, Sauer K. Biofilm dispersion. *Nat Rev Microbiol*. 2020;18(10):571-586. doi:10.1038/s41579-020-0385-0

57. Hehemann JH, Arevalo P, Datta MS, et al. Adaptive radiation by waves of gene transfer leads to fine-scale resource partitioning in marine microbes. *Nat Commun*. 2016;7:12860. doi:10.1038/ncomms12860

58. Tibbles BJ, Rawlings DE. Characterization of nitrogen-fixing bacteria from a temperate saltmarsh lagoon, including isolates that produce ethane from acetylene. *Microb Ecol*. 1994;27(1). doi:10.1007/BF00170115

59. D'Souza G, Waschina S, Pande S, Bohl K, Kaleta C, Kost C. Less is more: Selective advantages can explain the prevalent loss of biosynthetic genes in bacteria. *Evolution*. 2014;68(9):2559-2570. doi:10.1111/evo.12468

60. Mathis R, Ackermann M. Response of single bacterial cells to stress gives rise to complex history dependence at the population level. *Proc Natl Acad Sci USA*. 2016;113(15):4224-4229. doi:10.1073/pnas.1511509113

61. Brettin T, Davis JJ, Disz T, et al. RASTtk: A modular and extensible implementation of the RAST algorithm for building custom annotation pipelines and annotating batches of genomes. *Sci Rep*. 2015;5(1):8365. doi:10.1038/srep08365

62. Kanehisa M, Sato Y, Morishima K. BlastKOALA and GhostKOALA: KEGG Tools for Functional Characterization of Genome and Metagenome Sequences. *Journal of Molecular Biology*. 2016;428(4):726-731. doi:10.1016/j.jmb.2015.11.006

63. Cheng D, Jiang C, Xu J, Liu Z, Mao X. Characteristics and applications of alginate lyases: A review. *International Journal of Biological Macromolecules*. 2020;164:1304-1320. doi:10.1016/j.ijbiomac.2020.07.199

bioRxiv preprint doi: https://doi.org/10.1101/2023.07.14.548877; this version posted October 23, 2023. The copyright holder for this preprint (which was not certified by peer review) is the author/funder, who has granted bioRxiv a license to display the preprint in perpetuity. It is made available under aCC-BY-NC-ND 4.0 International license.

64. Zhang H, Yohe T, Huang L, et al. dbCAN2: a meta server for automated carbohydrate-active enzyme annotation. *Nucleic Acids Res*. 2018;46(W1):W95-W101. doi:10.1093/nar/gky418

65. NCBI Resource Coordinators. Database resources of the National Center for Biotechnology Information. *Nucleic Acids Res*. 2016;44(Database issue):D7-D19. doi:10.1093/nar/gkv1290

66. Altschul SF, Gish W, Miller W, Myers EW, Lipman DJ. Basic local alignment search tool. *J Mol Biol*. 1990;215(3):403-410. doi:10.1016/S0022-2836(05)80360-2

67. Almagro Armenteros JJ, Tsirigos KD, Sønderby CK, et al. SignalP 5.0 improves signal peptide predictions using deep neural networks. *Nat Biotechnol*. 2019;37(4):420-423. doi:10.1038/s41587-019-0036-z

68. Juncker AS, Willenbrock H, von Heijne G, Brunak S, Nielsen H, Krogh A. Prediction of lipoprotein signal peptides in Gram-negative bacteria. *Protein Sci*. 2003;12(8):1652-1662.

69. Andrews S. FastQC: A Quality Control Tool for High Throughput Sequence Data [Online]. Available online at: http://www.bioinformatics.babraham.ac.uk/projects/fastqc/. Published online 2010. http://www.bioinformatics.babraham.ac.uk/projects/fastqc/

70. Bolger AM, Lohse M, Usadel B. Trimmomatic: a flexible trimmer for Illumina sequence data. *Bioinformatics*. 2014;30(15):2114-2120. doi:10.1093/bioinformatics/btu170

71. Langmead B, Salzberg SL. Fast gapped-read alignment with Bowtie 2. *Nat Methods*. 2012;9(4):357-359. doi:10.1038/nmeth.1923

72. Danecek P, Bonfield JK, Liddle J, et al. Twelve years of SAMtools and BCFtools. *Gigascience*. 2021;10(2):giab008. doi:10.1093/gigascience/giab008

73. Liao Y, Smyth GK, Shi W. featureCounts: an efficient general purpose program for assigning sequence reads to genomic features. *Bioinformatics*. 2014;30(7):923-930. doi:10.1093/bioinformatics/btt656

74. Love MI, Huber W, Anders S. Moderated estimation of fold change and dispersion for RNA-seq data with DESeq2. *Genome Biology*. 2014;15(12):550. doi:10.1186/s13059-014-0550-8

75. Benjamini Y, Hochberg Y. Controlling the False Discovery Rate: A Practical and Powerful Approach to Multiple Testing. *Journal of the Royal Statistical Society: Series B (Methodological)*. 1995;57(1):289-300. doi:10.1111/j.2517-6161.1995.tb02031.x

76. Luo W, Brouwer C. Pathview: an R/Bioconductor package for pathway-based data integration and visualization. *Bioinformatics*. 2013;29(14):1830-1831. doi:10.1093/bioinformatics/btt285

77. Midani FS, Collins J, Britton RA. AMiGA: Software for Automated Analysis of Microbial Growth Assays. Silva-Rocha R, ed. *mSystems*. 2021;6(4):e00508-21. doi:10.1128/mSystems.00508-21